Quaternary Geochronology xxx (xxxx) xxx–xxx

Contents lists available at ScienceDirect

Quaternary Geochronology

journal homepage: www.elsevier.com/locate/quageo

Using a portable luminescence reader for rapid age assessment of aeolian sediments for reconstructing dunefield landscape evolution in southern Africa

A. Stone[a,*], M.D. Bateman[b], S.L. Burrough[c], E. Garzanti[d], M. Limonta[d], G. Radeff[d], M.W. Telfer[e]

[a] Department of Geography, The University of Manchester, M13 9PL, United Kingdom
[b] Department of Geography, University of Sheffield, Winter St., Sheffield, S10 2TN, United Kingdom
[c] School of Geography and the Environment, University of Oxford, South Parks Road, Oxford, OX1 3QY, United Kingdom
[d] Laboratory for Provenance Studies, Department of Earth and Environmental Sciences, Università Milano-Bicocca, 20126, Milano, Italy
[e] School of Geography, Earth and Environmental Sciences, Plymouth University, Drake Circus, Plymouth, Devon, PL4 8AA, United Kingdom

ARTICLE INFO

Keywords:
OSL dating
Portable luminescence reader (POSL)
Rapid age assessment
Dunefield dynamics
Aeolian sediments
Landscape evolution
Drylands
Quaternary environments

ABSTRACT

Analysis of sedimentary materials using a portable luminescence reader (or portable optically stimulated luminescence reader POSL), is a useful, rapid (a few minutes per sample), cost-effective and safe (not requiring exposure to chemicals) way to establish relative sample age. Moving beyond information that guides initial field interpretations, or develops targeted sampling strategies for full laboratory-based dating protocols, toward rapid age assessment has been more challenging. This study is the first demonstration of a simple, elegant and practical calibration of POSL signals into sample age estimates. This involved measuring the POSL signals from 144 samples with established published ages from across southern Africa, and a regression analysis. The data show that a regional-specific approach to calibration is needed, with regional patterns in POSL signals that are supported by 148 further undated samples. Four broad regions are defined: the Namib Sand Sea (NSS), the northern Kalahari (barchan dunes on the floor of Makgadigadi) (Nnk-MBa), the western Kalahari (WK) and the southern Kalahari (SK). Sample composition data, such as quartz-to-feldspar ratios (Q/F) appears to account for the largest contrasts within the dataset, whilst inherent POSL signal brightness and grain coloured-coatings (iron and clay) may also influence signals. The strength of the regressions (R^2 of 0.99, 0.93, 0.81 and one moderate at 0.52 for the NSS, SK, WK and NnK-MBa respectively) between POSL signals and sample age, (for ages back to 118, 104 74 and 5 ka for the NSS, SK, WK and NnK-MBa respectively), demonstrates the practicality and huge value of this simple approach. The implication is that region-specific calibrations must be built prior to using the POSL reader for rapid age assessments. This approach is a cost and time-effective method for inter-dunefield landscape-scale analyses, which will cast light on the key climatic variables driving landscape change in sand-rich drylands during the Late Quaternary, and also has the potential for large-scale analysis within other geomorphic settings.

1. Introduction

Reconstructing the landscape evolution of desert dunefields over the Late Quaternary helps to elucidate the mechanisms driving changes in key climate variables, such as precipitation, moisture balance and the wind. This understanding, coupled with using the Quaternary proxy datasets to test the robustness of numerical climate model simulations of dune-field dynamics, facilitates better model simulations that can be used to predict future changes and remobilisations (e.g. Thomas et al., 2005; Mayaud et al., 2007). However, using chronostratigraphies to reconstruct past environmental, and possibly climatic, response at the dunefield scale is both extremely time consuming and resource intensive when undertaking laboratory-based luminescence dating protocols, due to the large number of samples needed to overcome noise inherent in the preservational record (Stone and Thomas, 2008; Telfer et al., 2010; Bailey and Thomas, 2014). Therefore, the ability to make rapid age assessment of sediment burial ages using a portable optically stimulated luminescence reader (POSL) would be extremely useful.

The POSL approach offers a very quick (a few minutes per sample), first-order estimate of sample burial age that can: (1) aid the *in situ* interpretation of sites (e.g. Sanderson et al., 2003, 2007), (2) guide targeted field sampling, and (3) inform strategies for selecting samples

* Corresponding author.
E-mail address: abi.stone@manchester.ac.uk (A. Stone).

https://doi.org/10.1016/j.quageo.2018.03.002
Received 28 November 2017; Received in revised form 6 March 2018; Accepted 8 March 2018

to measure using laboratory-based luminescence dating protocols following fieldwork. In addition, this approach offers the possibility of producing large numbers of age estimates for a region, based on first calibrating the POSL signals of archived samples which also have published ages using full laboratory-based luminescence dating protocols (e.g. Stone et al., 2015 for initial samples from the Namib Sand Sea). Obtaining thousands of ages (POSL-derived), as opposed to the hundreds of ages available for the most rigorously dated dunefields, such as southern Africa's continental dunefields (Thomas and Burrough, 2016) or central Australia (Fitzsimmons et al., 2013), is key to accurate and useful reconstructions of past dune-field dynamics (Stone and Thomas, 2008; Telfer et al., 2010; Bailey and Thomas, 2014). Even though the POSL-derived ages are lower fidelity they are likely to give an adequate picture to assess changes at the landscape-scale, because sampling density may outweigh the importance of the precision of individual estimates. There were similar aims behind the laboratory-based standardised growth curve (SGC) approach, proposed by Roberts and Duller (2004) and applied to dunes by Telfer et al. (2008) and Yang et al. (2011). The SGC approach has the benefit of chemical sample refinement and a test dose to correct for differences in natural signal intensity arising from differences in sample mass or intrinsic luminescence brightness, but doesn't offer information in the field. Munyikwa and Brown (2014) combined use of the POSL and SGC approach, gamma-irradiating bulk sample material in the laboratory to produce a POSL-based SGC.

This study provides the first calibration tool for translating the POSL signals from samples into an estimate of burial age for selected continental dunefields within southern Africa (Fig. 1), and the only such approach worldwide. This is based on the analysis of 144 samples using the POSL for which there are published SAR-protocol (Murray and Wintle, 2000) based ages: 64 samples from linear dunes and lunettes near Witpan, in the southern Kalahari (SK) (Telfer and Thomas, 2006, 2007), 36 samples from linear dunes in the western Kalahari (WK) (Stone and Thomas, 2008), 18 samples from barchan dunes on the surface of Makgadikgadi pans (MBa), in the middle of the northern Kalahari (NnK) (Burrough et al., 2012; Burrough and Thomas, 2013) and 26 samples from complex linear dunes in the Namib Sand Sea (NSS) (Bristow et al., 2007; Stone et al., 2010; Stone et al., 2015). This study aims to establish whether one regression model for all southern African aeolian sediments would be appropriate (and perform well), or whether there are region-specific patterns, requiring their own regression models. In doing so, this study also aims to use sand petrology and mineralogy from each region to investigate the role of sample composition on POSL luminescence behaviour.

2. Methods

This study uses groups of samples that have established OSL age estimates using fully-prepared quartz and established laboratory protocols (Supp Info Table S1), which cover a wide proportion of southern Africa's continental dunefields (Fig. 1) Further details of sampling locations and analytical details of the SAR-protocols applied for dating the quartz fractions can be found in each of the individual papers listed at the end of section 1.

Archived bulk material from each of the samples (144 samples for which there published OSL ages, and a further 148 samples without published ages) (Supp Info 1)) was accessed and measured using the POSL reader developed by the Scottish Universities Environmental Research Centre (SUERC) (Sanderson and Murphy, 2010) in the luminescence laboratory setting (under subdued red-light or orange-light conditions at the Universities of Oxford and Sheffield). We aimed to keep the POSL protocol simple to enable its application in a field set up. For this reason we covered the base of the 5 cm petri dish with an even layer of bulk sediment, as opposed to weighing every sample to a specified mass. For subsamples that were weighed this amounts to ~5 g and we estimate this sample size equates to 60,000 grains for grain sizes

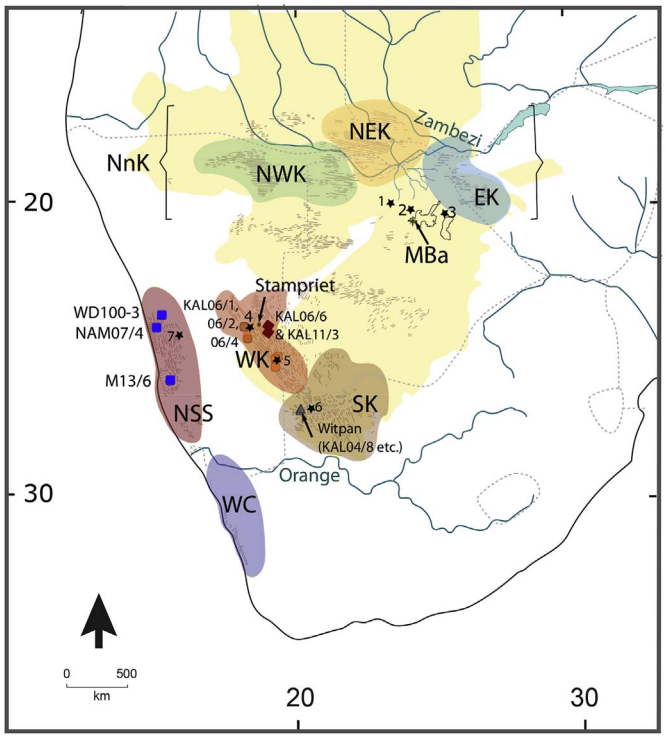

Fig. 1. Map of southern Africa, showing sampled locations, and ringed areas to show the INQUA dune database regional categorisation of southern African dunefields (figure modified after Thomas and Burrough, 2016). NSS = Namib Sand Sea, WC = west coast duefield, SK = southern Kalahari, WK = western Kalahari, NnK = northern Kalahari region depicted in brackets (made up of NK = north Kalahari, NEK = north-east Kalahari, EK = eastern Kalahari and MBa = Makgadikgadi barchans). The 7 labelled stars indicate locations for which additional sediment composition (petrology and heavy mineral) data is available from nearby sites for comparison with composition data from each of our studied regions (1 = Toteng, 2 = near Nwtetwe, 3 = Nata, 4 = Anib Lodge, 5 = Terra Rouge, 6 = Bokspit, 7 = Solitaire).

of 250–400 μm, (Bateman et al., 2015; Stone et al., 2015). We used a sequence of 15 s background dark count, followed by 60 s infra-red stimulation (IRSL) (LEDs centred around 880 ± 40 nm, and signals filtered with RG780 long pass filters), another 15 s background dark count, followed by 60 s of blue light stimulation (BLSL) (LEDs centred around 470 ± 20 nm, and signals filtered with CG420 long pass filters), and a final background dark count. Background subtraction from the first second of IRSL and BLSL signals used the average counts over the last 5 s (see method A in Stone et al. (2015). This is considered to be more appropriate than using total counts over 60 s, given the difference in shine-down rates between samples, and the particularly slow rate in NSS samples (see Stone et al., 2015). For the majority of samples there was sufficient material to run three subsample repeats and calculate an average (examples of the spread between subsamples can be seen from the open circles on the POSL signal-depth plots in Fig. 2).

In order to determine the ability of the POSL readings to give accurate predictions of sample ages, linear regression models using ordinary squares least regression were generated for the entire dataset and regional subsets. We report the coefficient of determination (R^2) and root mean square error (RMSE) as key measures of the goodness-of-fit and error of prediction, respectively (Table 1). P-values demonstrate that the reported results are significant at the 99% level. In order to assess prediction error on unseen data, a cross-validated estimate of the RMSE was generated using k-fold cross-validation (k = 10). Regression was undertaken in R (R Core Team, 2016) with cross-validation implemented in the DAAG (Data Analysis and Graphics) package (Maindonald and Bruan, 2015) (Table 1). This statistical significance approach is used, as opposed to leaving out 10% of the samples with which to 'predict' ages from the regression models and compare with

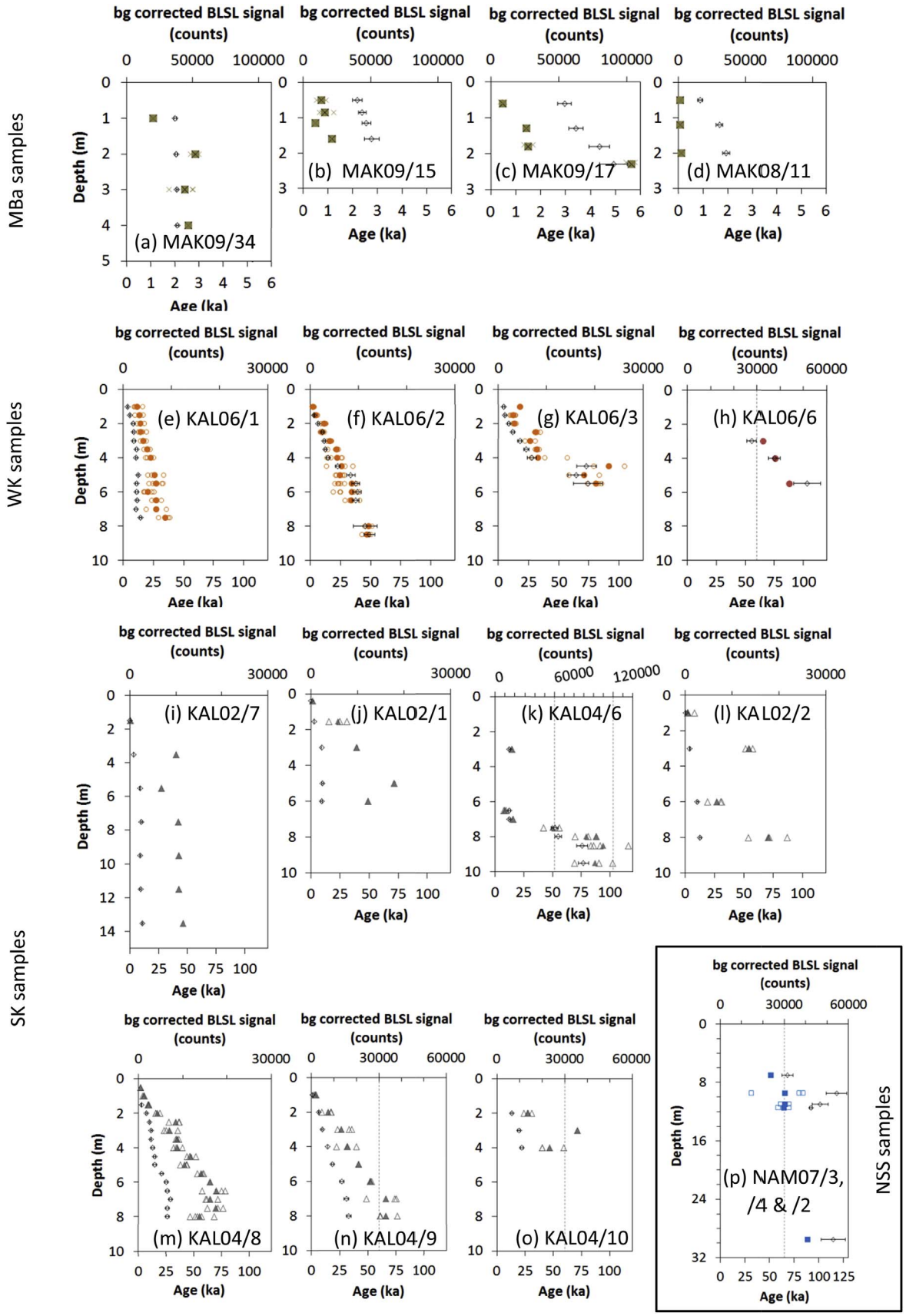

Fig. 2. Age-depth plots using published OSL ages (open diamonds) and age-P-OSL BLSL signal from (a–c) the Makgadigadi Barchans (MBa) (where filled crossed squares are averages and crosses are repeat measurements), (e–h) western Kalahari (WK) (where filled circles are averages and open circles are repeat measurements), (i–o) Witpan linear dunes in the SK (where filled triangles are averages and open triangles are repeat measurements), and (p) Narabeb site in the Namib Sand Sea NSS) (where filled squares averages and open squares are repeat measurements).

Table 1
Summary statistics for linear regression models.

Sample region	Age Range (ka)	n	Regression model parameters		Model fitting statistics			
			Slope	Intercept	r^2	RMSE (ka)	p-value	Cross validated RMSE (years) *
All data	0–120	144	0.61	8619	0.33	21.5	3.25×10^{-14}	21,880
NnK								
MBa	0–5	18	0.02	1881	0.52	0.8	4.35×10^{-4}	817
WK								
WK excluding east of Stampriet	0–75	36	2.32	3587	0.81	10.8	2.20×10^{-16}	11,079
SK								
Witpan	0–100	64	0.74	3315	0.93	5.8	3.95×10^{-15}	6130
NSS	0–120	26	2.85	83	0.99	4.0	2.20×10^{-16}	4724

*generated using k-fold cross-validation implemented in the DAAG (Data Analysis and Graphics) package (Maindonald and Bruan, 2015).

established ages (c.f. Stone et al., 2015), because the regression model benefits from using all of the available data.

The mineralogy of samples from each region was analysed at the Laboratory for Provenance Studies at the Università Milano-Bicocca, Italy, to compare sample composition between regions, and identify any potential influences on the POSL signals. These are also compared against existing minerological data from other sites in the southern African region (labelled as black stars in Fig. 1 and as italicised sample labels in Table 2). Samples of around 100 g were split for petrographic analysis (quartz, feldspar and lithic fragments) using araldite impregnated thin sections and mounting of grains > 2.9 g/cm^3 for heavy mineral identification (see Supp Info 2 for further methodological details).

3. Results and discussion

3.1. POSL signal depth plots

Within the dataset 16 vertical profiles are available to compare POSL signal depth plots with age-depth plots (Fig. 2), demonstrating the utility of the POSL reader to rapidly generate down core relative age profiles (c.f. Bateman et al., 2015) for ages back to ~120, 100, 75 and 5 ka for the NSS, SW, WK and Nnk-MBa respectively. For simplicity and clarity, and because the MBa samples have very low IRSL signals, we present the BLSL from the POSL (Fig. 2) (IRSL signals plots are available in Supp Info 3). We note that POSL signals cannot be assumed to be entirely mineral-specific as the diodes are stimulating bulk material (without chemical pre-treatment). The IRSL signal is likely to result from the feldspars in the bulk signal, owing to fact that quartz fast component shows little response to IR stimulation < 125 °C (Jain and Singhvi, 2001; Thomsen et al., 2008). The POSL BLSL signal is likely to be quartz-dominated, with some contribution from feldspar, particularly if the 60 s of IRSL stimulation has not emptied all the BLSL sensitive traps in the feldspar grains (see Munyikwa and Brown, 2014 for a more detailed investigation). In addition, any semi-opaque grain coatings (iron and clay) may also influence the luminescence signal behaviour of unrefined (as-found bulk sediment) using the POSL.

POSL BLSL signals show increases with depth (Fig. 2). Minor exceptions include small underestimates at 6 m in KAL06/1 (Fig. 2e), at 5 m in KAL06/2 (Fig. 2f), at 4, 5, 7 and 8 m in KAL04/8 (Fig. 2 m), a larger underestimate at 1.5 m in MAK09/15 (Fig. 2b) and small overestimates at 1 and 2.5 m in KAL06/3 (Fig. 2g) and 2 m in MAK09/34 (Fig. 2a) and larger overestimates at 2.5 m in KAL04/8 (Fig. 2m), at 3 m in KAL04/10 (Fig. 2o), at 5 m in KAL02/1 (Fig. 2j), at 3 m in KAL02/2 (Fig. 2l). The age inversion within profile at the Narabeb site in the NSS at 9.5 m is not reflected in average POSL BLSL, although this sample has the greatest range of values in the triplicate subsamples (Fig. 2p).

3.2. Regional regressions

If all southern African aeolian samples are considered together there is no significant relationship between POSL BLSL signals and sample age (Fig. 3, Table 1), with an R^2 of 0.33, for this dataset where ages range from 0.08 to ~120 ka. However, as Fig. 3 illustrates there are strong region-specific relationships between POSL BLSL signal and sample age within the dataset, and Table 1 gives the summary statistics for the linear regression models. For simplicity, comparability to Stone et al. (2015), and because the MBa samples contain very low IRSL signals, we consider the BLSL signals as the current best relative dating tool (and Supp Info Fig. 3.2, shows the IRSL signal v. age relationship). The contribution of feldspar to quartz-dominated POSL BLSL signals is explored in section 3.3.

The Namib Sand Sea (NSS) regression presented here (filled, blue squares, Fig. 3) of n = 26, with ages ranging from ~1 ka to ~120 ka, contains five new samples in the 2–6 ka range from Warsaw Dune (Bristow et al., 2007), and 6 samples not used in the regression within Stone et al. (2015). This yields the same gradient (to 1 significant figure) as previously calculated in the smaller dataset (Stone et al., 2015) and a change in the intercept from −147 to + 83. The western Kalahari (WK) samples (filled, orange circles, Fig. 3) define a POSL BLSL to age relationship that is fairly similar to that for the NSS (for sample ages spanning ~3 to 75 ka). However, there are three samples within the WK that appear to be outliers (filled, red diamonds, Fig. 3), and these are from a dune (KAL06/6) just east of Stampriet (Fig. 1) (three ages of 55.3, 75.1 and 103.2 ka). This unanticipated regional subdivision within WK is supported by 103 samples without published ages, in a plot of BLSL v. IRSL (Fig. 4), which shows distinct groupings (east of Stampriet - open, red diamonds; other parts of the WK - open, orange circles). The Witpan samples in the SK (filled, grey triangles) have brighter POSL-BLSL signals with increasing sample age compared to the NSS and WK samples, whilst MBa samples (green crosses) have the brightest POSL-BLSL signals per sample age within the dataset (Fig. 3).

The coefficient of determination is strongest for the NSS regression model (R^2 of 0.99), whilst SK and WK regression models have R^2 of 0.93 and 0.81 respectively (all significant at the 99% level). The MBa samples have a moderately good coefficient of determination (R^2 of 0.52), suggesting caution in using the model for age prediction. As per Table 1, errors on age predicted from POSL BLSL signals, generated using k-fold cross-validation (k = 10) suggest NSS age estimates have a cross validated RMSE of 4 ka (for ages up to ~120 ka), SK of 6 ka (for ages up to ~100 ka), WK of 11 ka (for ages up to ~75 ka), and NnK-MBa 0.8 ka (for ages up to ~5 ka).

3.3. Regional patterns in POSL signal behaviour

The clear regional patterns in the ratios of IRSL to BLSL signals from the POSL reader (Fig. 4) casts some light over the regional-specific

Table 2
Sample POSL summary data and sample composition summary data (see Fig. 1 for location of individual data points within each region).

Sample region and site	POSL			Petrological characteristics					Heavy Mineral abundance as% bulk sample weight							
	BLSL (bg corrected)	IRSL (bg corrected)	IRSL/BLSL	Classification	Q/F	% Q	% KF	% Plag	Zircon	Tourm	Rutile	Epidote	Garnet	Staur	Amphibole	Clinopyrox
NnK																
Mak barchans	455,416 ± 886	2611 ± 77	0.006	Qtzose	52	93	1.5	0.3	–	–	–	0.2	–	–	–	0.1
*Nata**	NA	NA	NA	Qtzose	11	91	4.4	4.1	–	–	–	–	–	–	–	–
*Near Nwtetwe**	NA	NA	NA	Pure Qtzose	66	98	0.6	0.9	–	–	–	–	–	–	–	–
*Toteng**	NA	NA	NA	Pure Qtzose	163	99	0.0	0.6	–	–	–	–	–	–	–	–
WK																
E of Stamp																
KAL06/6/1	32,467 ± 248	476 ± 41	0.015	Q-r, F-Qtzose	10	89	8.4	0.6	–	0.1	0.1	0.4	–	–	–	–
KAL06/6/3	43,877 ± 291	1023 ± 59	0.023	Q-r, F- Qtzose	10	88	8.3	0.3	0.1	0.1	0.1	0.4	–	0.1	–	–
KAL11/3/1	1240 ± 47	28 ± 11	0.023	Q-r, F- Qtzose	7	87	11.9	0.6	–	0.1	0.1	0.6	–	–	0.1	–
elsewhere																
KAL06/1/1	2880 ± 70	146 ± 23	0.051	Q-r, F- Qtzose	5	82	15.9	1.9	–	–	–	0.9	–	0.1	0.2	0.1
KAL06/2/2	1129 ± 49	68 ± 16	0.060	Q-r, F- Qtzose	6	85	12.1	2.3	0.1	–	–	0.5	–	–	0.1	–
KAL06/4/2	4548 ± 110	458 ± 37	0.101	Q-r, F- Qtzose	5	83	15.4	0.8	0.1	0.1	–	0.6	–	–	0.2	–
*Anib Lodge**	NA	NA	NA	Q-r, F- Qtzose	7	86	10.2	2.3	–	–	–	0.4	–	–	–	–
*Terra Rouge 1**	NA	NA	NA	Q-r, F- Qtzose	6	83	13.2	1.8	–	–	–	0.1	–	0.1	–	–
*Terra Rouge 2**	NA	NA	NA	Qtzose	10	89	8.2	0.9	–	0.1	–	0.2	–	0.2	–	–
KAL11/2/1	7285 ± 118	724 ± 47	0.099	Q-r, F- Qtzose	5	82	14.7	1.9	–	0.1	–	0.3	0.1	0.1	–	–
SK																
KAL04/8	1160 ± 480	56,460 ± 454	0.078	Q-r, F- Qtzose	9	86	7.5	2.2	0.1	–	–	0.5	0.1	–	–	–
*Bokspit**	NA	NA	NA	Quartzose	10	88	8.0	1.2	–	–	–	0.1	–	–	–	–
NSS																
NAM07/4/1	23,811 ± 480	56,460 ± 454	2.371	Q-r, F- Qtzose	3	70	12.8	9.7	–	–	–	–	0.1	–	–	1.2
WD 100-3	1451 ± 108	3159 ± 106	2.178	NA	NA	NA	NA	NA	NA	NA	NA	NA	NA	–	–	NA
M13/6	735 ± 75	1691 ± 72	2.301	Q-r, F- Qtzose	4	71	2.7	7.2	–	–	–	–	0.2	–	NA	2.7
*Solitaire 1**	NA	NA	NA	litho-F- Qtzose	2	61	13.9	11.7	0.2	–	0.1	0.2	0.3	–	0.5	0.9
*Solitaire 2**	NA	NA	NA	F-rich F- Qtzose	4	75	8.4	8.6	–	–	0.1	0.1	0.2	–	0.2	0.4
*Solitaire 3**	NA	NA	NA	F-rich F- Qtzose	3	70	11.0	9.7	0.1	–	–	0.2	0.1	–	0.2	0.4
*Solitaire 4**	NA	NA	NA	litho-F- Qtzose	3	64	8.6	11.4	0.1	–	–	0.3	0.2	–	0.2	0.6

*Italicised** are reference samples close to sites within each of our sampled regions (locations in Fig. 1).
Qtzose = quartzose, Q-r = quartz-rich, F-Quartzsose = feldspatho-quartzose, litho-F-Qtzose = litho-feldspatho-quartzose.
Q = quartz, F = feldspar.
% KF (potassium feldspar), % Plag (plagioclase) as volume percentage relative to bulk sediment.
Only HM with > 0.1% abundance as bulk sample weight are listed in the table.

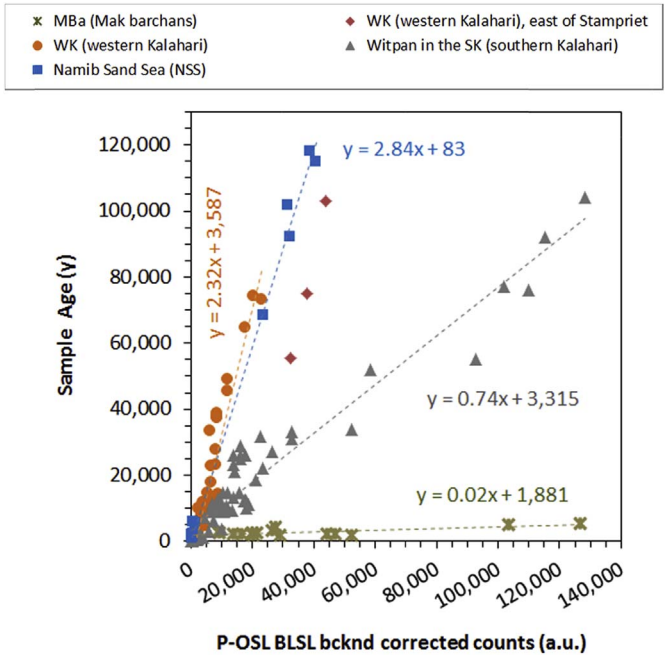

Fig. 3. Sample ages (established) regressed against POSL-BLSL signals, demonstrating the region-specific relationships for each region (see Table 1 for further summary statistics on the fit of these regression models).

calibrations of the POSL-BLSL signals to sample ages (Fig. 3). NSS samples (squares) have very bright IRSL signals compared to all other sites, whilst NnK-MBa (crosses) have low IRSL signals (Fig. 4, where open symbols represent POSL data from additional samples without established OSL ages). This reflects the petrological data from samples analysed within these two regions: NSS are 10–23% feldspar, 61–70% quartz and Q/F = 2 to 4, whilst NnK-MBa is 2% feldspar, 93% quartz and Q/F = 52 (Table 2). From these data, we can infer that POSL BLSL signals from NnK-MBa are very much quartz-dominated, whilst NSS samples will have the greatest additional signal from feldspar. Samples from SK (triangles) and the WK (circles and diamonds) represent an intermediate group, with as much compositional variability within the two regions and between them (Q/F = 5 to 10, with 82–89% quartz and 9–18% feldspar) (Table 2), suggesting something other than quartz and feldspar abundance might drive the differences in their POSL BLSL signals v. age relationship (Fig. 3). We note that there is some separation between the POSL IRSL v. BLSL signals for the sub-region east of Stampriet in the WK (diamonds) from the rest of the WK (circles) and SK (triangles) (Fig. 4) that is not captured by the petrological dataset (Table 2), and that this supports treating this sub-region separately in the sample age POSL BLSL signal regressions (Fig. 3).

Other factors controlling the patterns seen in the POSL BLSL v. age regressions (Fig. 3) may include: local dose rates; inherent sample luminescence sensitivity (which is not corrected for using the POSL), and the degree of grain-coatings on the sands (Sanderson and Murphy, 2010; Lomax et al., 2007). Dose rates for the NnK-MBa samples have a mean of 1.00 ± 0.17 Gy (1 s.d.), whilst the mean for WK is 1.43 ± 0.11 Gy, for SK (Witpan) is 1.39 ± 0.15 Gy, and for the NSS is 1.60 ± 0.27 Gy (Supp. Info 1). Therefore, whilst the low dose rates for NnK-MBa and higher dose rates for NSS compared to other regions might indicate some link with POSL sensitivity, this factor does not account for the different patterns seen between SK and WK (and within WK) (Figs. 3 and 4).

In terms of inherent luminescence sensitivity, MBa samples (in the NnK) give very bright POSL BLSL signals for their age, compared to the other regions (Figs. 2 and 3), although the high Q/F ratios and low dose rates for this region also contribute to this trend. From their setting, the NnK-MBa sediments will have been through multiple transport cycles through the Okavango and Makgadikgadi pans systems, which can make the quartz luminescence signal more sensitive (e.g. Moska and Murray, 2006). Laboratory measurements of OSL from bulk (untreated) samples per unit dose for a subset of samples from each region, using a RISØ reader, give an insight into bulk sample inherent sensitivity (see Supp. Info. 4 for experimental details). Whilst any feldspar will also contribute to the blue-LED stimulated OSL signals of these aliquots, the ratio of this contribution to L_x and T_x is constant for each aliquot, which means L_x/T_x values are useful as comparators between samples and regions. This shows the NSS has the lowest values, suggesting the luminescence sensitivity of the bulk sediment per unit dose is the lowest for this region (Fig. S4). Nnk-MBa samples have higher values than most of the SK and WK samples, with the exception of the subset of the WK-east of Stampriet, which, on average, has slightly higher values (Fig. S4). The bulk-sample luminescence sensitivity proxy provided by these L_x/T_x values may be (i) an additional factor driving the rapid increase in POSL BLSL with sample age for NnK-MBa (green crosses, Fig. 3) (additional to higher Q/F ratios) and (ii) a factor driving the higher POSL BLSL signal per sample age in the subset of WK east of Stampriet (red diamonds) compared to the rest of the WK (orange

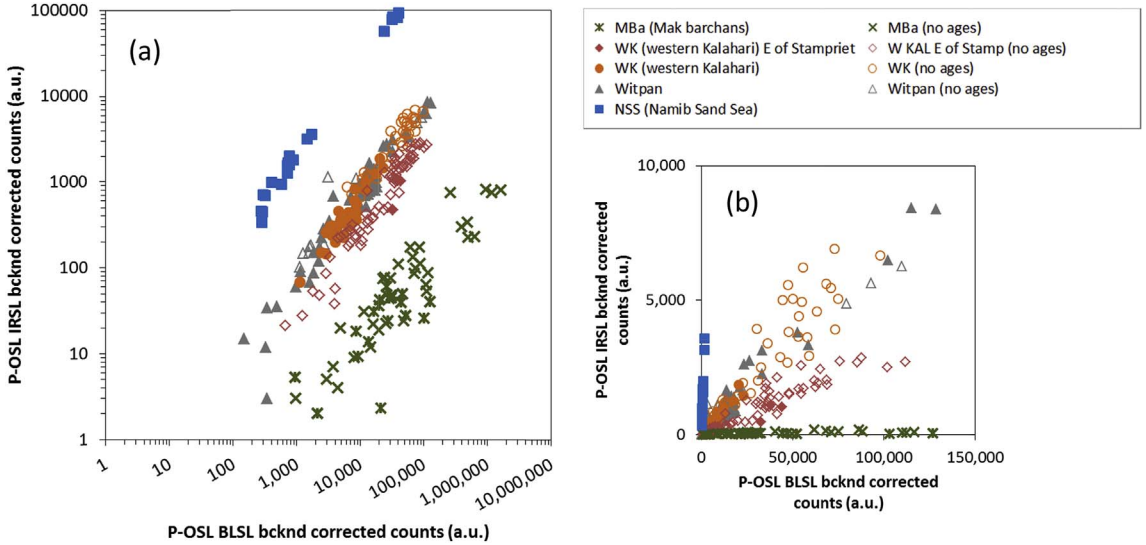

Fig. 4. BLSL against IRSL signals from the POSL for samples from each region, showing (a) the whole dataset as a log-log plot and (b) an inset for signals < 10,000 IRSL and < 150,000 BLSL to illustrate the separation the populations of western Kalahari samples to the west and to the west of Stampriet.

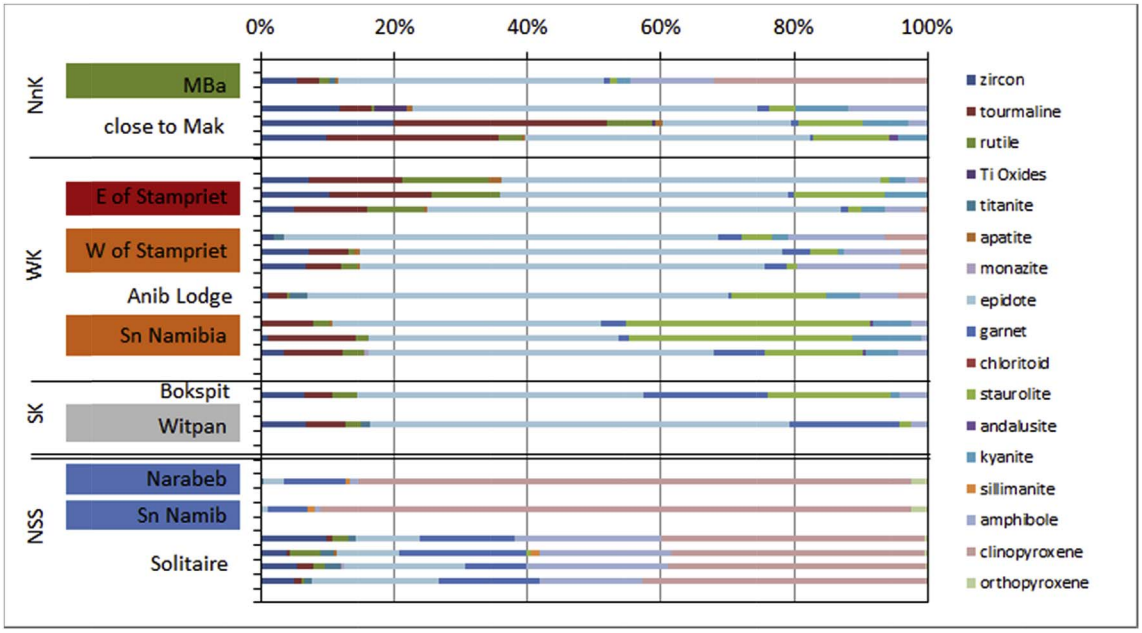

Fig. 5. Sample composition, showing proportions of heavy minerals present (see Table 2 for an idea of heavy mineral abundance as % weight of the bulk sample). Close to Mak = Nata, near Nwtetwe, Toteng. Also west of Stampriet = Anib Lodge, Sn Nambia = Terra Rouge 1 & 2 and KAL12/1, N Cape = Bokspit site (see Fig. 1).

circles) (Fig. 3). Future investigations could isolate quartz OSL sensitivity from the influence of feldspar-derived BLSL using the 'OSL IR depletion ratio' approach of Duller (2003) or by measuring mineral-specific separates.

Heavy mineral assemblages within these samples may relate to both sample provenance and diagenesis (Fig. 5, Table 2), and in turn may reflect differences in quartz sensitivity relating to source region and the number of transport cycles. There is clear compositional difference between the NSS and the Kalahari, with greater abundance of clinopyroxene and amphibole, typically more garnet, and far less tourmaline and rutile in the former (Fig. 5). Within the Kalahari the NnK-MBa sample is unique with significant percentage of clinopyroxene. WK samples east of Stampriet stand out from the rest of the WK, containing higher % of zircon, tourmaline and rutile. Further work could also investigate whether HMs have any direct influence on POSL signals, by stimulating HM separates.

There are different degrees of grain coatings (iron and clay) between the regions studied. Using Munsell colour, the stand-out feature is the absence of red coating on NnK-MBa samples, compared to all other samples (Supp Info 1). The NSS sample colour hues are all 7.5 YR, WK are 2.5 YR or 5 YR and the SK samples are more variable (2.5 YR, 5 YR and 7.5 YR) (Supp Info 1). POSL signal depletion indices (ratio of first 30 s to last 30 s of stimulation) (Sanderson and Murphy, 2010) may provide an insight into the influence of grain coatings, expecting cleaner grain surfaces to have higher depletion indices (more rapid signal depletion), if all other things are equal (Sanderson, pers. comm). However, samples with no grain coatings (NnK-MBa) are not differentiated by their POSL IRSL depletion indices (Supp Info Table S1 and Fig. S5A), suggesting a lack of measurable influence of grain coatings on POSL signals. The trend in POSL BLSL depletion indices (Figs. S5A and B) track the identified marked regional differences in Q/F ratios, where samples with lower Q/F ratios (more feldspar) have higher IRSL/BLSL ratios and lower BLSL depletion indices (Fig. S5B).

3.4. Extending the application of this approach

This southern African dataset demonstrates that region-specific calibrations of POSL signal data to (established) sample age have great potential to provide a rapid age assessment approach for new sample sites within those regions. This could be particularly useful in the assessment of sediment accumulation histories at a large spatial scale, where the transport of many hundreds of samples for laboratory sample is logistically and financially challenging, and involves time-intensive laboratory analysis. The technique is well suited to application within other aeolian settings, and fluvial-settings could also be tested. In taking this approach forward (in the context of this study and beyond) we propose some recommendations, based on what we have learned from this dataset, and expect further guidelines to emerge with the collection of further regional datasets.

(i) In producing an initial calibration dataset (stage 1), sample size should be sufficient that adding samples does not notably alter the regression model. Samples should cover the full-range of anticipated ages (profile top, middle, bottom), and a range of locations within the region. See discussion in section 3.2 about the minimal influence of increasing sample size for the NSS region. However, it seems prudent to further populate regional regressions where n is small (NSS n = 26 and NnK-MBa n = 18). The luminescence sensitivity per unit dose of the quartz OSL signal (for age) and the sensitivity of the bulk sediment sample (for POSL-BLSL) should be characterised.

(ii) In producing rapid-age estimates for new field samples from the regional regressions (stage 2) it is important to confirm that samples conform to characteristics of that regional regression using POSL parameters, such as IRSL/BLSL ratios (as an indicator of Q/F ratios), and POSL signal depletion indices. It would also be sensible to retrospectively put a subset of samples through laboratory luminescence analysis to characterise luminescence sensitivity, alongside these same analyses for stage 1 calibration data. Finally, a useful procedural control will be to put ~5% of stage 2 samples through the same full laboratory OSL dating protocol, chosen to span age range and a range of locations, to confirm they fit the regional regression model being used. The differences between the WK and SK dataset demonstrate the importance of this final step.

Whilst not the focus of this paper, these data show that POSL IRSL/BLSL ratios act as proxies for Q/F ratios to first order, and this rapid- and field-derived data has useful potential to help identify changes in

sediment provenance, or character (weathering and removal of feldspars) in the field.

4. Conclusions

POSL signals from 144 sand dune samples across southern Africa for which there are established published OSL ages reveal excellent relative age information, as shown by POSL signals plotted by depth (Fig. 2), and the strength of regressions between POSL signals and established, published ages confirms that signals reflect sample age (Fig. 3). The dataset demonstrates that regional-specific regressions models are needed, and that the predictive power of these model for the four regions is strong for Namib Sand Sea (NSS) ($R^2 = 0.99$), Witpan in the SK ($R^2 = 0.93$) and the western Kalahari (WK) ($R^2 = 0.81$) and moderate for barchan dunes in Makgadikgadi (NnK-MBa) ($R^2 = 0.52$) (for ages back to ~120, 100, 75 and 5 ka respectively) (Table 1, Fig. 3). The error on ages predicted from POSL BLSL signals, generated using k-fold cross validation, demonstrates the utility of this rapid age approach (Table 1, (Fig. 3). Whilst there are four distinct regional regression models, there are only three distinct regional groups in terms of petrological and heavy mineral composition (NSS, WK + SK and NnK-MBa) (Table 2, Fig. 5). It is likely that Q/F ratios drive the broad differences in POSL BLSL signal v. age (Fig. 3) between NSS (Q/F 2 to 4), the WK + SK (Q/F of 5–10) and the NnK-MBa (Q/F of 52). There is no clear evidence that grain coatings (iron and clay) influence the regional patterns in POSL signals (Fig. S4). An additional control is inherent POSL signal brightness, and bulk sediment luminescence sensitivity per unit dose experiments on a RISØ reader show that samples from NnK-MBa have L_x/T_x values that are, on average, around double those for the NSS, and that the WK east of Stampriet has higher L_x/T_x on average (with only one overlapping value) than the rest of the WK region, which may help account for the intra-region variability in POSL BLSL signal v. age (Fig. 3).

Notwithstanding the complexities outlined around the influence of grain coatings and inherent POSL signal brightness, the strength of the regressions between POSL BLSL signals and sample age for each region (Table 1), demonstrates that this is an excellent and hugely valuable approach to rapid age assessment. It provides an approach that is elegant and simple to use in the field, noting that the lead in of a producing a region-specific calibration is required. The calibrations of POSL signals into first order age estimates allows the production of a large number of low-fidelity ages for a dunefield (in the field, or in the lab) quickly (< 5 min per sample) cheaply and with no chemical exposure (a significant safety advantage). This approach has great potential to provide new insights into the large-scale sedimentary dynamics of dunefields through the Late Quaternary not only allowing the identification of chronostratigraphic breaks and hiatuses and changes in sedimentary material at the site-scale (Bateman et al., 2015; Sanderson et al., 2003; Sanderson and Murphy, 2010; Leighton et al., 2013), but enabling larger inter-dunefield landscape-scale analyses, previously precluded because of the heavy monetary and time cost.

Acknowledgements

This research utilised samples collected as part of other projects and the reader is directed toward the acknowledgement of those papers for information regarding the relevant research/collecting permits. A.S. thanks W. Fletcher for guidance with regression model statistics, J. Durcan, G. King, and R. Smedley and attendees of LED 2017 in Cape Town for productive discussions around the POSL reader and this dataset. A.S. also thanks the two reviewers for their insightful and constructive comments on the POSL approach and manuscript.

Appendix A. Supplementary data

Supplementary data related to this article can be found at http://dx.doi.org/10.1016/j.quageo.2018.03.002.

References

Bailey, R.M., Thomas, D.S.G., 2014. A quantitative approach to understanding dated dune stratigraphies. Earth Surf. Process. Landforms 39, 614–631.
Bateman, M.D., Stein, S., Ashurst, R.A., Selby, K., 2015. Instant Luminescence Chronologies? High resolution luminescence profiles using a portable luminescence reader. Quat. Geochronol. 30, 141–146.
Bristow, C.S., Duller, G.A.T., Lancaster, N., 2007. Age and dynamics of linear dunes in the Namib Desert. Geology 35, 555–558.
Burrough, S.L., Thomas, D.S.G., 2013. Central southern Africa at the time of the African Humid Period: a new analysis of Holocene palaeoenvironmental and palaeoclimate data. Quat. Sci. Rev. 80, 29–46.
Burrough, S.L., Thomas, D.S.G., Bailey, R.M., Davies, L., 2012. From landform to process: morphology and formation of lake-bed barchan dunes, Makgadikgadi Botswana. Geomorphology 161–162, 1–14.
Duller, G.A.T., 2003. Distinguishing quartz and feldspar in single-grain luminescence measurements. Radiat. Meas. 37, 161–165.
Fitzsimmons, K.E., Cohen, T.J., Hesse, P.P., Jansen, J., Nason, G.C., May, J.-H., Barrows, T.T., Haberlah, D., Hilgers, A., Kelly, T., Larsen, J., Lomax, J., Treble, P., 2013. Late Quaternary palaeoenvironmental change in the Australian drylands. Quat. Sci. Rev. 74, 78–96.
Jain, M., Singhvi, A.K., 2001. Limits to depletion of blue-green light stimulated luminescence in feldspars: implications for quartz dating. Radiat. Meas. 33, 883–892.
Leighton, C.L., Thomas, D.S.G., Bailey, R.M., 2013. Allostratigraphy and Quaternary dune sediments: not all bounding surfaces are the same. Aeolian Res. 11, 55–60.
Lomax, J., Hilgers, A., Twidale, C.R., Bourne, J.A., Radtke, U., 2007. Treatment of broad palaeodose distributions in OSL dating of dune sands from the western Murray Basin, South Australia. Quat. Geochronol. 2, 51–56.
Maindonald, J., Bruan, W.J., 2015. DAAG: Data Analysis and Graphics data and functions (R package version 1.22). http://CRAN.R-project.org/package=DAAG.
Mayaud, J.R., Bailey, R.M., Wiggs, F.S., 2017. Modelled responses of the Kalahari Desert to 21st century climate and land use. Nat. Sci. Rep. 7, 3887. http://dx.doi.org/10.1038/s41598-017-04341-0.
Moska, P., Murray, A.S., 2006. Stability of the quartz fast-component in insensitive samples. Radiat. Meas. 41, 878–885.
Munyikwa, K., Brown, S., 2014. Rapid equivalent dose estimation for eolian dune sands using a portable OSL reader and polymineralic standardised luminescence growth curves: expedited sample screening for OSL dating. Quat. Geochronol. 22, 116–125.
Murray, A.S., Wintle, A.G., 2000. Luminescence dating of quartz using an improved single-aliquot regenerative-dose protocol. Radiat. Meas. 32, 57–73.
R Core Team, 2016. R: a Language and Environment for Statistical Computing. R Foundation for Statistical Computing, Vienna, Austria.
Roberts, H.M., Duller, G.A.T., 2004. Standardised growth curves for optical dating of sediment using multiple-grain aliquots. Radiat. Meas. 38, 241–252.
Sanderson, D.C.W., Murphy, S., 2010. Using simple portable OSL measurements and laboratory characterisation to understand complex and heterogeneous sediment sequences for luminescence dating. Quat. Geochronol. 5, 299–305.
Sanderson, D.C.W., Bishop, P., Stark, M.T., Spencer, J.Q., 2003. Luminescence dating of anthropogenically reset canal sediments from Angkor Borei, Mekong Delta, Cambodia. Quat. Sci. Rev. 22, 1111–1121.
Sanderson, D.C.W., Bishop, P., Stark, M., Alexander, S., Penny, D., 2007. Luminescence dating of canal sediments from angkor borei, mekong delta, Southern Cambodia. Quat. Geochronol. 2, 322–329.
Stone, A.E.C., Thomas, D.S.G., 2008. Linear dune accumulation chronologies from the southwest Kalahari, Namibia: challenges of reconstructing late Quaternary palaeoenvironments from aeolian landforms. Quat. Sci. Rev. 27, 1667–1681.
Stone, A.E.C., Thomas, D.S.G., Viles, H.A., 2010. Late Quaternary palaohydrological changes in the northern Namib Sand Sea: new chronologies using OSL dating of interdigitated aeolian and water-lain interdune deposits. Palaeogeogr. Palaeoclimatol. Palaeoecol. 288, 35–53.
Stone, A.E.C., Bateman, M.D., Thomas, D.S.G., 2015. Rapid age assessment in the Namib Sand Sea using a portable luminescence reader. Quat. Geochronol. 30, 134–140.
Telfer, M.W., Thomas, D.S.G., 2006. Complex Holocene lunette dune development, South Africa: implications for palaeoclimate and models of pan development in arid regions. Geology 34 (10), 853–856.
Telfer, M.W., Thomas, D.S.G., 2007. Late Quaternary linear dune accumulation and chronostratigraphy of the southern Kalahari: implications for aeolian palaeoclimatic reconstructions and predictions of future dynamics. Quat. Sci. Rev. 26, 2617–2630.
Telfer, M.W., Bateman, M.D., Carr, A.S., Chase, B.M., 2008. Testing the applicability of a standardized growth curve (SGC) for quartz OSL dating: Kalahari dunes, South African coastal dunes and Florida dune cordons. Quat. Geochronol. 3, 137–142.
Telfer, M.W., Bailey, R.M., Burrough, S.L., Stone, A., Thomas, D.S.G., Wiggs, G.S.F., 2010. Understanding linear dune chronologies: insights from a simple accumulation model. Geomorphology 120, 195–208.
Thomas, D.S.G., Burrough, S.L., 2016. Luminescence-based dune chronologies in southern Africa: analysis and interpretation of dune database records across the subcontinent. Quat. Int. 401 (Part B), 30–45.
Thomas, D.S.G., Knight, M., Wiggs, G.F.S., 2005. Remobilization of southern African desert dune systems by twenty-first century global warming. Nature 435, 1218–2121.
Thomsen, K.J., Jain, M., Murray, A.S., Denby, P.M., Roy, N., Bøtter-Jensen, L., 2008. Minimizing feldspar OSL contamination in quartz UV-OSL using pulsed blue stimulation. Radiat. Meas. 43, 752–757.
Yang, L., Lai, Z.P., Long, H., Zhang, H., 2011. Construction of a quartz OSL standardised growth surve (SGC) for aeolian samples from the Horqin dunefield in northeastern China. Geochronometria 38, 391–396.